Anomalous Spin-Orbit Field via the Rashba-Edelstein Effect at the W/Pt Interface

Shutaro Karube,[1,2,*] Nobuki Tezuka,[1,2] Makoto Kohda,[1,2,3] and Junsaku Nitta[1,2,3]

[1] *Department of Materials Science, Graduate School of Engineering, Tohoku University, Sendai, Japan*

[2] *Center for Spintronics Research Network, Tohoku University, Sendai, Japan*

[3] *Center for Science and Innovation in Spintronics (Core Research Cluster) Organization for Advanced Studies, Tohoku University, Sendai, Japan*

(Received 5 June 2019; revised manuscript received 30 October 2019; accepted 20 December 2019; published 6 February 2020)

We study the spin-orbit (SO) field in $Ni_{80}Fe_{20}$(Permalloy; Py)/W/Pt trilayer by means of spin-torque ferromagnetic resonance, and demonstrate that the W/Pt interface generates an extra SO field that acts on the Py layer. This unprecedented field originates from the following three processes: (1) spin accumulation at the W/Pt interface via the Rashba–Edelstein effect, (2) diffusive spin transport in the W layer, and (3) spin absorption into the Py layer through accumulation at the Py/W interface. Our results mean that we can create an extra SO field away from the ferromagnet/metal interface and control its strength by a combination of two different metals.

DOI: 10.1103/PhysRevApplied.13.024009

The spin-orbit (SO) field or torque generated by the spin Hall effect (SHE) [1] from SO materials can effectively perform magnetization switching of an adjacent ferromagnetic layer [2–5]. The SO field is based on a spin current density, $\mathbf{J}_S^{int}$, acting on a ferromagnet (FM) interface [6,7]:

$$\mathbf{J}_S^{int} = \mathrm{Re}G_{\uparrow\downarrow}(\mathbf{m}\times\boldsymbol{\mu}\times\mathbf{m}) + \mathrm{Im}G_{\uparrow\downarrow}(\mathbf{m}\times\boldsymbol{\mu}). \quad (1)$$

Here, $G_{\uparrow\downarrow}$, $\boldsymbol{\mu}$, and $\mathbf{m}$ are spin-mixing conductance at the FM interface, the vector of spin accumulation, and the unit vector of magnetization in the FM layer, respectively. This accumulation, $\boldsymbol{\mu}$, is necessary for generating the SO torque on the magnetization, $\mathbf{m}$. The first and second terms in Eq. (1) correspond to dampinglike (DL) and fieldlike (FL) torques, respectively. If the accumulation, $\boldsymbol{\mu}$, is modulated, we can manipulate the magnitude of the SO torques.

Previously, heavy metals, such as Pt, Ta, and W, with strong SO coupling have been intensively studied with respect to various aspects, e.g., the SO-torque-induced switching, domain wall displacement [8], spin relaxation [9,10], and controllable SO torque [11,12], for fundamental physics and spintronics applications. Moreover, it is found that surface states of topological insulators and Rashba states at interfaces can also generate SO torque or spin current via the Edelstein effect [13–20], resulting in effective magnetization switching because of their giant SO torque [21–23]. Thus, the magnitude of SO torque in various materials are systematically investigated and unveiled. For further efficiency of the SO torque or extra SO torques, alternative SO materials are desired both in research and in practical applications.

Recently, there have been several approaches for synthesizing SO materials. One such approach is by using oxides, such as CuO_X [24,25], WO_X [26], and PtO_X [27,28]. The spin-orbit torque generation of these materials is believed to originate from the Rashba-Edelstein (RE) effect. Through the introduction of oxygen, there can be an enhancement of the torque relative to that of the pure metal, or the torque can be controlled via ionic-oxygen conduction by gating. Another approach is a SO heterojunction consisting of heavy metals (HMs), such as in sandwich structures [29] and bilayers [30]. Concerning sandwich structures (HM1/FM/HM2), the generated SO torque would be enhanced due to double-spin accumulation at the top and bottom FM interfaces originating from the heavy metals, which have opposite signs of the spin Hall angle relative to each other, for example, Pt and Ta [31,32]. These reports suggest that we can design SO materials by such combinations. In the case of bilayers, generated SO torque succeeds in performing field-free switching in W/Pt/$Co_{40}Fe_{40}B_{20}$/MgO structures [30]. Thus, the challenges in synthesizing SO materials are important for spintronics applications in the future. Based on previous reports regarding the RE effect [15,20,33], we have the possibility to generate an extra SO field in the ferromagnet far from the HM interface with diffusive spin transport in the HM layer. Here, we demonstrate an additional SO field from the W/Pt interface.

*karube@material.tohoku.ac.jp

We prepare the multilayer films by means of dc and rf magnetron sputtering at room temperature with the following reference samples: $Ni_{80}Fe_{20}$(Py, 5)/W(2)/AlO_X (2), Py(5)/W(1−5)/Pt(1), Py(5)/W(2)/Pt(1−4), Py(4–7)/W(2)/AlO_X(2), Py(4–7)/Pt(1), Py(5)/Pt(1)/AlO_X(2), Py(5)/Pt(1)/W(2)/Mg(1.5) (values in parentheses indicate the thickness in nanometers; Py, Permalloy). Here, AlO_X, and Mg, which is naturally oxidized, are employed as capping layers for the prevention of oxidation. According to x-ray diffraction measurements, all metallic films are polycrystalline. Next, devices for spin-torque ferromagnetic resonance (ST FMR) [34] are fabricated by conventional lift-off processes using e-beam lithography and Ar-ion milling. For ST FMR measurements, we apply rf currents in the range of 3–14 dBm in power and 5–12 GHz in frequency from a signal generator into the devices, and detect dc voltages via anisotropic magnetoresistance (AMR) rectification, while applying a static magnetic field, H, of up to 290 mT.

First, we demonstrate the generation of the extra SO field in the Py layer via the RE effect at the W/Pt interface. A schematic image is shown for the stacking structure and spin-current generation in Fig. 1(a). Figure 1(b) shows the detected DL fields, H_{DL}, divided by the applied current density, J_C, in the case of Py(5)/W(2)/AlO_X(2), Py(5)/Pt(1), and Py(5)/W(2)/Pt(1) at 6 dBm and 8 GHz of rf current using Eq. (2) [25]. The detected voltage can be described as $V_{\mathrm{mix}} = V_S L(H) + V_A \partial L(H)/\partial H$, with the Lorentzian $L(H)$ as a function of the magnetic field H, the amplitude of the Lorentzian V_S, and the amplitude of the derivative Lorentzian V_A, and cannot be used for comparison due to different values of several parameters, such as the applied rf current I_{rf}, AMR amplitude ΔR, and the half width at half maximum of the ST FMR spectrum $\mu_0 \Delta H$ in each sample:

$$\mu_0 H_{\mathrm{DL}} = \frac{2V_S}{I_{\mathrm{rf}} \Delta R} \frac{2\sqrt{2}\pi f\, \mu_0 \Delta H (2\mu_0 H_R + \mu_0 M_{\mathrm{eff}})}{\gamma (\mu_0 H_R + \mu_0 M_{\mathrm{eff}}) \mu_0 H_R}. \quad (2)$$

Here, γ, f, $\mu_0 H_R$, $\mu_0 M_{\mathrm{eff}}$ are the gyromagnetic ratio for electrons, applied frequency, resonance field, and effective magnetization. As for the cases of Py/W and Py/Pt, the signs of the detected DL fields are in good agreement with previous reports [4,31] for both cases. In our case of 1-nm-thick Pt, there is insufficient spin relaxation in the Pt layer, according to the spin-diffusion length of Pt: $\lambda_{\mathrm{sf}}^{\mathrm{Pt}} = (1.0 \pm 0.1)$ nm, which we measure, meaning the V_{mix} amplitude is smaller than that originating from the saturated spin Hall angle in the case of a Pt layer thicker than $\lambda_{\mathrm{sf}}^{\mathrm{Pt}}$. So, if there is only bulk contribution to the generation of the DL field, we should see a summation between W and Pt that includes a decay of the spin current in the W layer because of spin relaxation. Since the DL field from the 1-nm-thick Pt layer is quite small, the DL field in the case of the Py/W/Pt trilayer should be approximately the same as that in the Py/W case. However, the amplitude for Py/W/Pt seems to be reduced. This implies that there is another contribution generating the extra SO field, as shown in the red curve in Fig. 1(b). Moreover, we measure a control sample consisting of Py(5)/W(2)/Cu(5)/Pt(1) multilayer, with Cu insertion between the W and Pt layers, as shown in Fig. 1(c). The extra component disappears in this case, which indicates the importance of the W/Pt interface. This behavior is similar to that in another report regarding the disappearance of SO fields upon Cu insertion between a ferromagnet and Pt [35]. We also check the contribution of the Pt/AlO_X interface via the RE effect, as

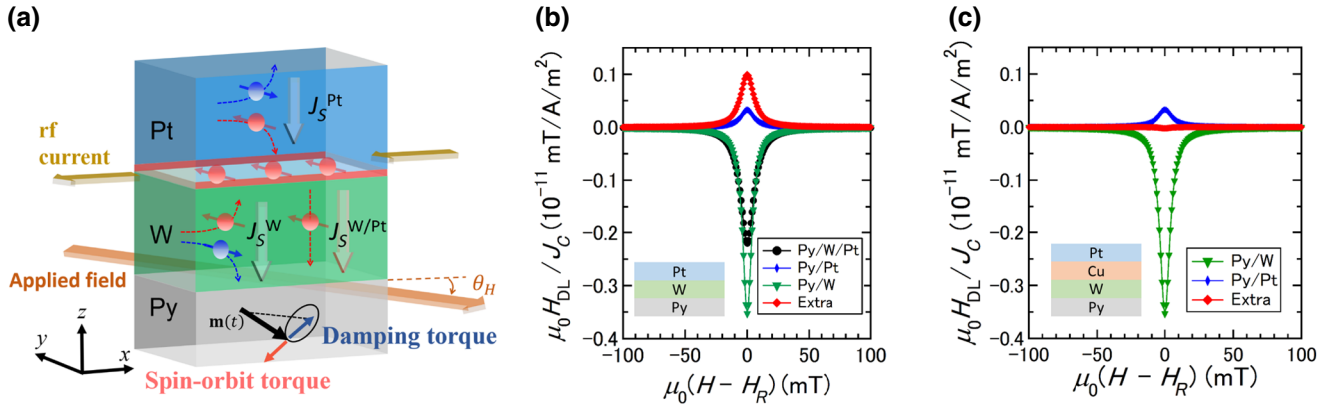

FIG. 1. (a) Schematic image showing each spin-current, J_S, generation via the spin Hall effect from the W and Pt layers and the RE effect from the W/Pt interface. During ST FMR, a magnetic field is applied at an angle θ_H to the strip, and the magnetization of the Py layer feels the spin-orbit torque. (b) The generated DL field divided by charge-current density, J_C, for Py(5 nm)/W(2 nm) (green triangles), Py(5 nm)/Pt(1 nm) (blue diamonds), and Py(5 nm)/W(2 nm)/Pt(1 nm) (black circles). Red diamonds correspond to the extra component of the DL field. (c) The generated DL field divided by charge-current density in the case of Py(5 nm)/W(2 nm)/Cu(5 nm)/Pt(1 nm).

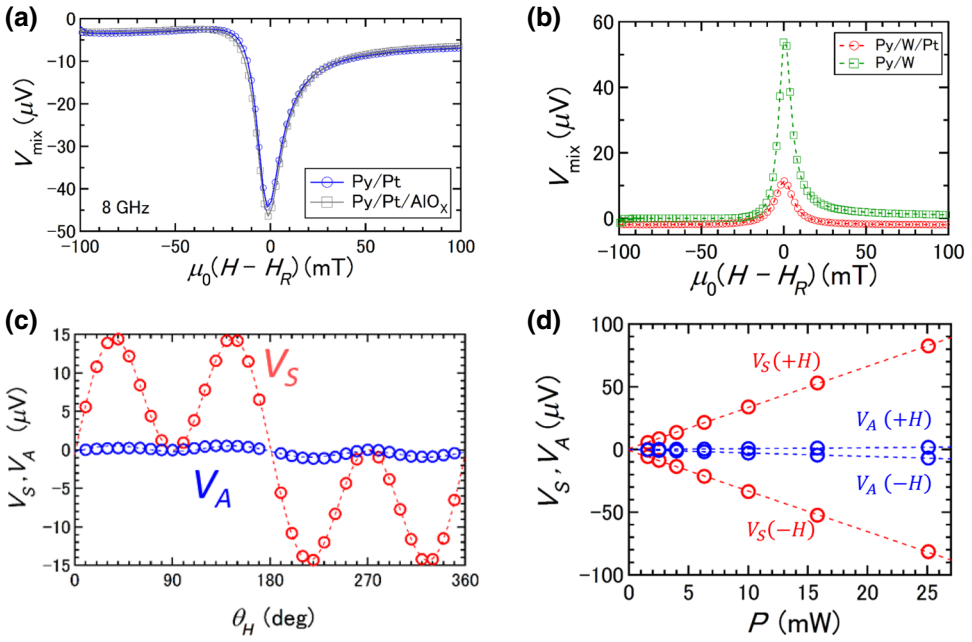

FIG. 2. (a) Detected voltages in the ST FMR measurement at 8 GHz for Py(5 nm)/Pt(1 nm) (blue open circles) and Py(5 nm)/Pt(1 nm)/AlO_X(2 nm) (gray open squares) with fitted curves. (b) Detected voltages in the ST FMR measurement at 8 GHz for Py(5 nm)/W(2 nm)/AlO_X(2 nm) (green open squares) and Py (5 nm)/W(2 nm)/Pt(1 nm) (red open circles). (c) Field-angular dependence of the symmetric (red open circles) and antisymmetric (blue open circles) voltages, and (d) rf power dependence of both voltages as a function of the applied field in the case of Py (5 nm)/W(2 nm)/Pt(1 nm).

shown in Fig. 2(a), by comparing it to the Pt-only sample and find that there is no difference between them, and thus, there is no contribution from the Pt/AlO_X interface. Accordingly, we investigate the DL fields generated from the W and Pt layers via the spin Hall effect and a negligible field from the Pt surface (or the Pt/AlO_X interface) via the RE effect. Therefore, this extra field should emerge from the W/Pt interface via the RE effect because it is not possible to explain it by the other contributions.

To confirm the origin of the extra SO field arising from the RE effect at the W/Pt interface, we focus on another SO field, i.e., the FL field. We investigate the ST FMR signal for the cases of Py(5)/W(2)/AlO_X(2) and Py(5)/W(2)/Pt(1) at 6 dBm and 8 GHz of rf current and, surprisingly, detect almost symmetric voltages in both cases, as seen in Fig. 2(b). To clarify these symmetric voltages, we investigate only Pt(1) or W(2)/AlO_X(2), while varying the Py thickness, and extract the DL and FL spin-torque efficiencies, ξ_{DL} and ξ_{FL}, respectively, based on Ref. [36]. The efficiencies are calculated to be $\xi_{DL}^{Pt} = 0.0244$, $\xi_{FL}^{Pt} = -0.0016$, $\xi_{DL}^{W} = -0.0427$, and $\xi_{FL}^{W} = 0.0167$ in the Py/W and Py/Pt systems. Concerning the 1-nm-thick Pt case, the positive value of ξ_{DL}^{Pt}, which is related to the effective spin Hall angle, is in good agreement with the reported value [34], with a consideration for the spin relaxation in Pt as $\xi_{DL} = \xi_{DL}^{0}[1 - \mathrm{sech}(t_{HM}/\lambda_{sf}^{HM})]$ [37], because this Pt thickness is the same as that of the spin-diffusion length of Pt: $\lambda_{sf}^{Pt} = (1.0 \pm 0.1)$ nm, which we measure. Negligible ξ_{FL}^{Pt} is also consistent with the previous report [34]. Concerning the 2-nm-thick W case, the negative sign of ξ_{DL}^{W} is consistent and the amplitude is close to that of a reported value for $\alpha - W$ [4]. The finite ξ_{FL}^{W} is in good agreement with the value for the W/CoFeB system [38]. From this analysis, the almost symmetric voltage in the Py(5)/W(2)/AlO_X(2) case is attributed to the finite FL field, which is comparable to that of the Oersted field from the W layer, but with the opposite sign, because the antisymmetric voltage, V_A, consists of a summation between the Oersted field and the FL field:

$$V_A \propto (H_{FL} + H_{Oe})\sqrt{1 + \frac{\mu_0 M_{eff}}{\mu_0 H_R}} = \left(\frac{\hbar}{2e}\frac{\xi_{FL} J_C}{\mu_0 M_S t_{FM}} + \frac{J_C t_{HM}}{2}\right)\sqrt{1 + \frac{\mu_0 M_{eff}}{\mu_0 H_R}}. \quad (3)$$

Next, we consider why we observe almost symmetric voltages in the ST FMR measurement of Py(5)/W(2)/Pt(1) as well. The amplitudes of the symmetric and antisymmetric voltages are related to the SO fields, including the DL, FL, and Oersted fields, as described in Eqs. (3) and (4) [36]:

$$V_S \propto H_{DL} = \frac{\hbar}{2e}\frac{\xi_{DL} J_C}{\mu_0 M_S t_{FM}}. \quad (4)$$

Here, e, $\hbar$, H_{DL}, H_{FL}, H_{Oe}, and J_C represent the elementary charge, Dirac constant, DL field, FL field, Oersted field, and charge-current density, respectively. V_A is almost negligible, which means that H_{FL} in the Py(5)/W(2)/Pt(1) system has a comparable amplitude and opposite sign to that of H_{Oe} from the W and Pt layers. In other words, $H_{FL}^{tot} = -(H_{Oe}^{W} + H_{Oe}^{Pt})$. This compensation is not unusual because we see a similar kind of signal in Py(5)/W(2)/AlO_X(2), where comparable FL and Oersted

fields emerge at the Py/W interface, i.e., $H_{\mathrm{FL}}^{\mathrm{W}} = -H_{\mathrm{Oe}}^{\mathrm{W}}$. If the Pt layer, instead of the AlO_X layer, creates an additional Oersted field in the Py layer, then the almost symmetric voltage should be broken and an antisymmetric voltage should appear, but the detected voltage is still symmetric. This is due to the contribution of the W/Pt interface for generating an extra effective FL field, i.e., $H_{\mathrm{FL}}^{\mathrm{W/Pt}} \approx -H_{\mathrm{Oe}}^{\mathrm{Pt}}$.

One possible concern is that these results come from a spin-pumping effect during FMR [39], which could explain the almost symmetric voltage in ST FMR measurements. To rule out this spin-pumping effect, we also measure the in-plane field-angular dependence of the signals and rf power dependence, as shown in Figs. 2(c) and 2(d), and find $\sin 2\theta_H \cos\theta_H$ behavior, which is attributed to the ST FMR signal [40], and a linear relationship between the detected voltage and power. This ensures that the ST FMR measurements and analysis are performed precisely and are reliable.

Now, we must consider how both the extra DL and FL fields can be created via the W/Pt interface. As stated previously, we propose that these results originate from the RE effect, which generates spin accumulation at the W/Pt interface. The RE effect has already been demonstrated in several systems, such as in the surface states of topological insulators [14,15] and Rashba interfaces [17–20,33,41–45], which have spin-split dispersion at the Fermi level. Therefore, the nonequilibrium-accumulated spins propagate with decay along the out-of-plane direction (through the W and Pt layers) diffusively. If the W thickness, t_{W}, is smaller or comparable to that of the spin-diffusion length of W, $\lambda_{\mathrm{sf}}^{\mathrm{W}} \approx (1.1 \pm 0.3)$ nm, as extracted and in good agreement with other reports [46,47], some portion of the accumulation can pass through the W layer and finally reach the Py/W interface. Then, the spin absorption and accumulation take place and the extra DL and FL fields emerge into the Py layer, separately from the SHE contribution.

Based on this assumption, we now focus on quantitative analysis to extract the anomalous SO fields. First, we calculate charge-current densities and Oersted fields in and from each layer, considering shunting effects and applied power of the rf current. The rf current injected into the devices depends on the strip impedance. So, an applied 6 dBm power is actually reduced by following the rf current power relationship, $P = [V/(R_I + R_S)]^2 R_S$, where P, V, R_I, and R_S represent the actual injected power, voltage, internal impedance of the signal generator, and impedance of the sample strip, respectively. The Oersted field from each layer can be simply estimated by $H_{\mathrm{Oe}}^{\mathrm{HM}} = J_C^{\mathrm{HM}} t_{\mathrm{HM}}/2$, which is introduced from the Gauss law in the case of an infinite conductive plane. The fields divided by the charge-current densities are shown in Fig. 3(a). We also estimate the conventional DL and FL fields from the bulk W and Pt layers from the following equation [36], with extracted $\xi_{\mathrm{DL}}^{\mathrm{HM}}$ and $\xi_{\mathrm{FL}}^{\mathrm{HM}}$ values based on the argument

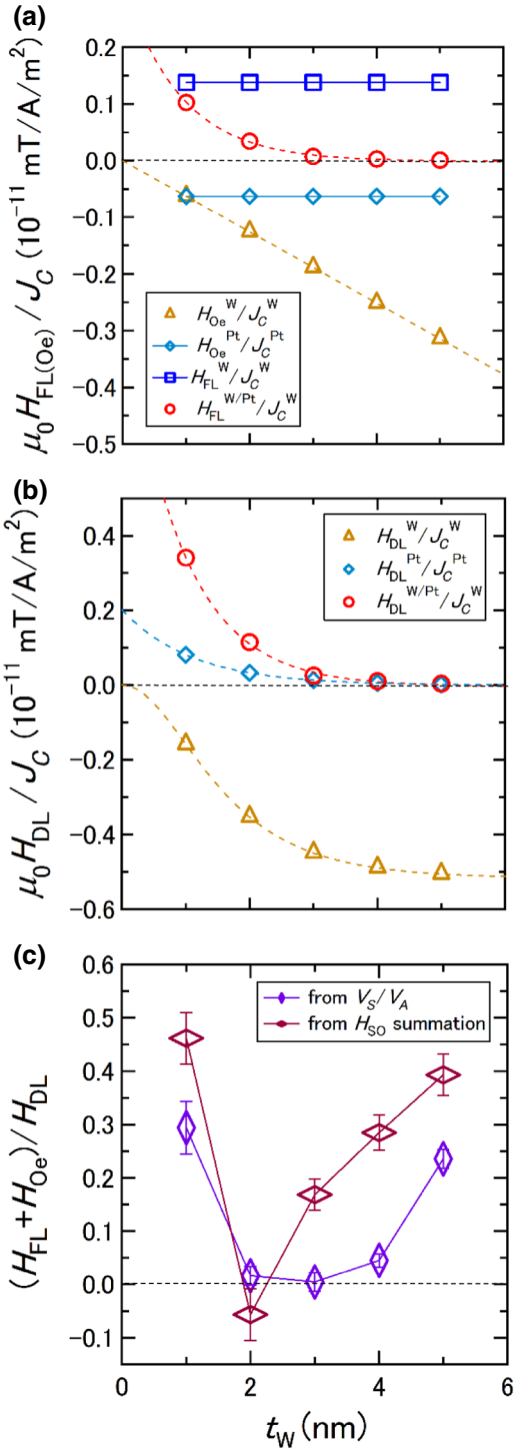

FIG. 3. (a) Estimated Oersted and FL fields divided by charge-current density, J_C, as a function of the W thickness in the cases of W(1–5 nm) bulk, Pt(1 nm) bulk, and W(1–5 nm)/Pt(1 nm) interface with spin diffusion in the W layer cases. (b) Estimated DL field divided by charge-current density, J_C, as a function of W thickness in the cases of Pt(1 nm) bulk, W(2 nm)/Pt(1 nm) interface with spin diffusion in the W layer, and W(1–5 nm) bulk. (c) Comparison of the field ratio $(H_{\mathrm{FL}} + H_{\mathrm{Oe}})/H_{\mathrm{DL}}$ as a function of W thickness for estimation from raw V_S/V_A data and from H_{SO} field summation.

above, as shown in Figs. 3(a) and 3(b):

$$H_{\mathrm{DL(FL)}} = \frac{\hbar}{2e}\frac{J_C^{\mathrm{HM}}}{\mu_0 M_S t_F}\xi_{\mathrm{DL(FL)}}. \tag{5}$$

To estimate the DL field from the W layer, we use $\xi_{\mathrm{DL}}^{\mathrm{W}} = \xi_{\mathrm{DL}}^{\mathrm{W},0}[1 - \mathrm{sech}(t_{\mathrm{W}}/\lambda_{\mathrm{sf}}^{\mathrm{W}})]$ based on the spin-diffusion model with $\lambda_{\mathrm{sf}}^{\mathrm{W}} \approx (1.1 \pm 0.3)$ nm, as obtained by us for the estimation. Moreover, for the DL field from the Pt layer, it has to propagate into the W layer with spin diffusion. Therefore, we assume a simple exponential decay [20,33] for the amplitude of the DL field, $H_{\mathrm{DL}}^{\mathrm{Pt}} = H_{\mathrm{DL}}^{\mathrm{Pt},0}\exp(-t_{\mathrm{W}}/\lambda_{\mathrm{sf}}^{\mathrm{W}})$. Here, $H_{\mathrm{DL}}^{\mathrm{Pt},0}$ stands for the DL field generated in the 1-nm-thick Pt layer before spin diffusion into the W layer. With these parameters, we can estimate the extra field contributions coming from the W/Pt interface by subtraction from the detected signal. According to Eq. (3), there is a cancellation of the fields between Py(5)/W(2) and Py(5)/W(2)/Pt(1):

$$H_{\mathrm{FL}}^{\mathrm{W/Pt}}\exp(-t_{\mathrm{W}}/\lambda_{\mathrm{sf}}^{\mathrm{W}}) = -H_{\mathrm{Oe}}^{\mathrm{Pt}}. \tag{6}$$

Here, $H_{\mathrm{FL}}^{\mathrm{W/Pt}}$ means the FL field generated by the W/Pt interface and is related to spin accumulation at the interface. By taking the value of the Oersted field from the Pt layer, the normalized FL field $H_{\mathrm{FL}}^{\mathrm{W/Pt}}$ divided by the charge-current density in the W layer is $H_{\mathrm{FL}}^{\mathrm{W/Pt}}\exp(-t_{\mathrm{W}}/\lambda_{\mathrm{sf}}^{\mathrm{W}})/J_C^{\mathrm{W}} = 0.034 \times 10^{-11}\,\mathrm{mT/A/m^2}$ for the 2-nm-thick W case. Here, the reason why we choose $J_{\mathrm{C}}^{\mathrm{W}}$ as the charge-current density for the calculation is that the W layer is dominant for conduction close to the W/Pt interface because of a lack of evidence of interfacial alloying, according to the phase diagram between W and Pt [48], and the energy difference between the surface binding energy of W, 10 eV [49], and the conventional sputtering energy, 2 eV [50]. The estimated FL field is comparable to that of the conventional FL field generated at the Py/W interface, which has the normalized FL field as $H_{\mathrm{FL}}^{\mathrm{W}}/J_C = 0.138 \times 10^{-11}\,\mathrm{mT/A/m^2}$ in this study. We also estimate the DL field $H_{\mathrm{DL}}^{\mathrm{W/Pt}}$ from the W/Pt interface based on Eq. (2):

$$\begin{aligned}&\mu_0 H_{\mathrm{DL}}^{\mathrm{W/Pt}}\exp(-t_{\mathrm{W}}/\lambda_{\mathrm{sf}}^{\mathrm{W}})\\ &= \frac{2V_S}{I_{\mathrm{rf}}\Delta R}\frac{2\sqrt{2}\pi f\,\mu_0\Delta H(2\mu_0 H_{\mathrm{R}} + \mu_0 M_{\mathrm{eff}})}{\gamma(\mu_0 H_{\mathrm{R}} + \mu_0 M_{\mathrm{eff}})\mu_0 H_R}\\ &\quad - \mu_0 H_{\mathrm{DL}}^{\mathrm{W}} - \mu_0 H_{\mathrm{DL}}^{\mathrm{Pt}}\exp(-t_{\mathrm{W}}/\lambda_{\mathrm{sf}}^{\mathrm{W}}),\end{aligned} \tag{7}$$

We now know the amplitudes of the DL fields from both W and Pt according to Eq. (7). Therefore, it is possible to estimate the extra contribution from the W/Pt interface, as shown in Fig. 3(b). Here, we also assume simple exponential decay [20,33], similar to the DL field from the Pt layer, and almost all current going through the W layer. Surprisingly, we find that the amplitude of the DL field seen in Fig. 3(b) is not negligible, but is comparable to the conventional DL field from the W layer in the case of thinner W thicknesses, such as 1 nm. This means that we can create extra SO fields in the FM layer away from the HM interface. Figure 3(c) shows the ratio of the effective fields derived from the V_S/V_A raw data [27] for comparison with the ratio calculated by a summation of extracted SO fields from the assumptions above:

$$\frac{H_{\mathrm{Oe}} + H_{\mathrm{FL}}}{H_{\mathrm{DL}}} = \frac{V_A}{V_S}\left(1 + \frac{\mu_0 M_{\mathrm{eff}}}{\mu_0 H_R}\right)^{-1/2}. \tag{8}$$

In spite of the presence of multiple SO field parameters, the ratio roughly follows the same behavior with respect to W thickness as that of the ratio from V_S/V_A, and thus, implies that our calculation is an accurate estimation. As for the minimum position at 2 nm, it is attributed to the spin-diffusion length (1.1 nm) of the W layer. Spin accumulation generated via the spin Hall effect in heavy metals or the RE effect at the W/Pt interface, regarding the SO fields, diffuses inside the W layer with decay. So, overall, the minimum appears at around 2 nm. Moreover, we also investigate the Pt thickness dependence of the extra DL field, as shown in Fig. 4. Here, we include the Pt thickness dependence of the DL torque efficiency of the Pt layer, $\xi_{\mathrm{DL}}^{\mathrm{Pt}}$, for the extra DL field calculation. As observed, it decays with increasing thickness. This decay length is roughly estimated to be $\lambda_{\mathrm{decay}} = (2.0 \pm 0.7)$ nm, which is nearly the estimated spin-diffusion length of Pt [$\lambda_{\mathrm{sf}}^{\mathrm{Pt}} = (1.0 \pm 0.1)$ nm]. This behavior is in good agreement with our assumption in this study that the generated spins from the RE effect at the W/Pt interface diffuse not only into the W layer, but also into the Pt layer. So, the amount of spins is reduced with increasing Pt thickness due to spin diffusion in the Pt layer.

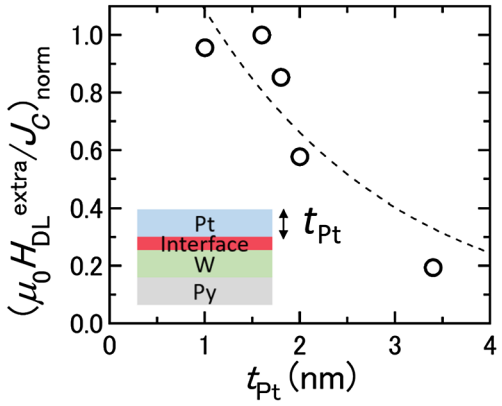

FIG. 4. Normalized DL field divided by charge-current density as a function of the Pt thickness.

Finally, we focus on an inverse stacking for W and Pt, by changing from Py/W/Pt to the Py/Pt/W trilayer. If the assumption in which the RE effect at the W/Pt interface contributes to the extra SO fields is true, we should see a difference in the $V_{\rm mix}$ signal because the inverse-stacking structure changes the direction of the effective electric field, and thus, a different direction of spin polarization also results via the Rashba effect, as shown in Fig. 5(a). We would expect to see the opposite sign of the additional FL field in the case of Py/Pt/W, as compared with Py/W/Pt. Thus, we also perform the measurement for Py/Pt/W with the same thickness conditions, and we show the experimental results for both cases in Fig. 5(b). As observed, the signal for inverse stacking has an antisymmetric voltage, which implies that there is a large change of the SO fields relative to that of the previous stacking case of Py/W/Pt. For a detailed calculation of the FL field $H_{\rm FL}^{\rm Pt/W}$ from the Pt/W interface in the case of a Py/Pt/W trilayer system, based on Ref. [25], we employ

$$\mu_0 H_{\rm FL}^{\rm Pt/W} \exp(-t_{\rm Pt}/\lambda_{\rm sf}^{\rm Pt}) = \frac{2V_A}{I_{\rm rf}\Delta R}\frac{\sqrt{2}\mu_0\Delta H(2\mu_0 H_R+\mu_0 M_{\rm eff})}{\mu_0 H_R+\mu_0 M_{\rm eff}} - \mu_0 H_{\rm Oe}^{\rm Pt} - \mu_0 H_{\rm Oe}^{\rm W}. \quad (9)$$

As mentioned above, we already know the amplitudes of the Oersted fields from the W and Pt layers. So, we can estimate the amplitude of $H_{\rm FL}^{\rm Pt/W}$ with subtraction, where we note that $H_{\rm FL}^{\rm Pt}$ is negligible based on the estimated quite small value of $\xi_{\rm FL}^{\rm Pt}$. The value of $H_{\rm FL}^{\rm Pt/W}$ divided by charge-current density in the W layer is calculated to be -0.0267×10^{-11} mT/A/m^2 for the 2-nm-thick W case. To estimate the field at the Pt/W interface, we have to consider exponential decay in the Pt layer, which has a spin-diffusion length of 1.0 nm, as estimated in the same way as that described in the above discussion. This amplitude is estimated to be -0.0730×10^{-11} mT/A/m^2. Taking into account decay in the W layer, which has a spin-diffusion length of 1.1 nm, we extract, in the case of Py/W/Pt, an amplitude of $H_{\rm FL}^{\rm W/Pt}/J_C^{\rm W}$ of 0.3170×10^{-11} mT/A/m^2.

We succeed in finding the opposite sign of the extra FL field between Py/W/Pt and Py/Pt/W systems due to the change in sign of the Rashba parameter through inverse stacking. However, the value for the Py/Pt/W case is four times smaller than that for the Py/W/Pt case. The reason for this is related to the FL torque efficiency at the Py/HM interface. Py/W and Py/Pt interfaces have finite and negligible values of $\xi_{\rm FL}^{\rm HM}$, respectively. This implies that there is a difference in the ability to accumulate spins at the interface for both cases. The Py/Pt interface cannot produce spin accumulation as effectively as that of Py/W. Thus, we do not see the same amplitude of the additional FL field. These experimental results ensure that this anomalous behavior comes from the RE effect at the W/Pt interface and the diffusive spin-transport process in the HM layers. Concerning further interfacial systems, we have to consider and calculate the electron density distribution and nuclei electric fields for the amplitude of the Rashba parameter [33]. Moreover, we have to seek the same sign of spin polarization between the spin Hall effect from heavy-metal layers and the RE effect. We expect that there are good combinations because of the many reported SO materials.

In conclusion, we study the Py/W/Pt trilayer system, by means of careful comparison of ST FMR measurements with several reference samples, and demonstrate the generation of extra SO fields via the RE effect at the W/Pt interface. We can create additional SO fields in the FM layer and control the amplitudes by a combination of HM layers, which include an interface far from the FM layer, and paves the way for more efficient and functional spintronic devices.

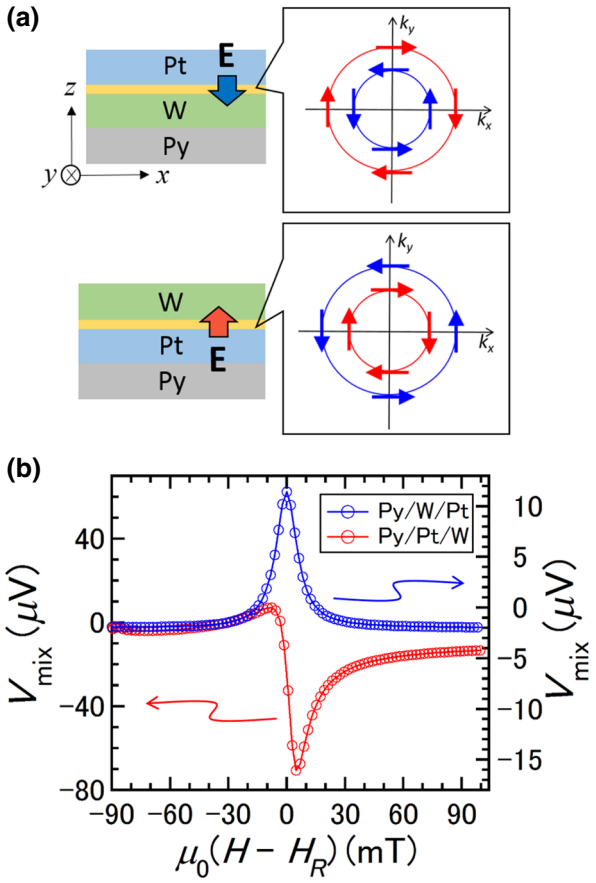

FIG. 5. (a) Cross-section views of structures with effective electric field E at the heavy-metal interface and expected Rashba spin polarization in the cases of normal stacking (Py/W/Pt) and inverse stacking (Py/Pt/W). (b) Detected voltages in the ST FMR measurement for Py(5 nm)/W(2 nm)/Pt(1 nm) and Py(5 nm)/Pt(1 nm)/W(2 nm).

ACKNOWLEDGMENTS

We thank Dr. J. Ryu, H. Gamou, R. Thompson, R. Ando, and S. Fujikawa for their helpful information and constructive discussions. This work is partially supported by the Japan Society for the Promotion of Science (JSPS) (Grants No. 15H05699, No. 17H06512, and No. 18K14111), the Center for Spintronics Research Network at Tohoku University, and the Center for Science and Innovation in Spintronics at Tohoku University.

[1] M. I. Dyakonov and V. I. Perel, Possibility of orientating electron spins with current, JETP Lett. **13**, 467 (1971).

[2] L. Liu, C.-F. Pai, Y. Li, H. W. Tseng, D. C. Ralph, and R. A. Buhrman, Spin-torque switching with the giant spin hall effect of tantalum, Science **336**, 555 (2012).

[3] L. Liu, O. J. Lee, T. J. Gudmundsen, D. C. Ralph, and R. A. Buhrman, Current-induced Switching of Perpendicularly Magnetized Magnetic Layers Using Spin Torque From the Spin Hall Effect, Phys. Rev. Lett. **109**, 096602 (2012).

[4] C.-F. Pai, L. Liu, Y. Li, H. W. Tseng, D. C. Ralph, and R. A. Buhrman, Spin transfer torque devices utilizing the giant spin Hall effect of tungsten, Appl. Phys. Lett. **101**, 122404 (2012).

[5] Q. Hao and G. Xiao, Giant Spin Hall Effect and Switching Induced by Spin-Transfer Torque in a $W/Co_{40}Fe_{40}B_{20}/MgO$ Structure with Perpendicular Magnetic Anisotropy, Phys. Rev. Appl. **3**, 034009 (2015).

[6] Y.-T. Chen, S. Takahashi, H. Nakayama, M. Althammer, S. T. B. Goennenwein, E. Saitoh, and G. E. W. Bauer, Theory of spin Hall magnetoresistance, Phys. Rev. B **87**, 144411 (2013).

[7] A. Brataas, Y. V. Nazarov, and G. E. W. Bauer, Finite-Element Theory of Transport in Ferromagnet–Normal Metal Systems, Phys. Rev. Lett. **84**, 2481 (2000).

[8] S. Emori, U. Bauer, S. M. Ahn, E. Martinez, and G. S. Beach, Current-driven dynamics of chiral ferromagnetic domain walls, Nat. Mater. **12**, 611 (2013).

[9] J. Ryu, M. Kohda, and J. Nitta, Observation of the D'yakonov-Perel' Spin Relaxation in Single-Crystalline Pt Thin Films, Phys. Rev. Lett. **116**, 256802 (2016).

[10] H. Gamou, J. Ryu, M. Kohda, and J. Nitta, Different spin relaxation mechanisms between epitaxial and polycrystalline Ta thin films, Appl. Phys. Express **10**, 023003 (2017).

[11] E. Lesne, Y. Fu, S. Oyarzun, J. C. Rojas-Sanchez, D. C. Vaz, H. Naganuma, G. Sicoli, J. P. Attane, M. Jamet, E. Jacquet, J. M. George, A. Barthelemy, H. Jaffres, A. Fert, M. Bibes, and L. Vila, Highly efficient and tunable spin-to-charge conversion through Rashba coupling at oxide interfaces, Nat. Mater. **15**, 1261 (2016).

[12] R. Mishra, F. Mahfouzi, D. Kumar, K. Cai, M. Chen, X. Qiu, N. Kioussis, and H. Yang, Electric-field control of spin accumulation direction for spin-orbit torques, Nat. Commun. **10**, 248 (2019).

[13] V. M. Edelstein, Spin polarization of conduction electrons induced by electric current in two-dimensional asymmetric electron systems, Solid State Commun. **73**, 233 (1990).

[14] A. R. Mellnik, J. S. Lee, A. Richardella, J. L. Grab, P. J. Mintun, M. H. Fischer, A. Vaezi, A. Manchon, E. A. Kim, N. Samarth, and D. C. Ralph, Spin-transfer torque generated by a topological insulator, Nature **511**, 449 (2014).

[15] K. Kondou, R. Yoshimi, A. Tsukazaki, Y. Fukuma, J. Matsuno, K. S. Takahashi, M. Kawasaki, Y. Tokura, and Y. Otani, Fermi-level-dependent charge-to-spin current conversion by Dirac surface states of topological insulators, Nat. Phys. **12**, 1027 (2016).

[16] Y. Wang, P. Deorani, K. Banerjee, N. Koirala, M. Brahlek, S. Oh, and H. Yang, Topological Surface States Originated Spin-Orbit Torques in Bi_2Se_3, Phys. Rev. Lett. **114**, 257202 (2015).

[17] J. C. Sanchez, L. Vila, G. Desfonds, S. Gambarelli, J. P. Attane, J. M. De Teresa, C. Magen, and A. Fert, Spin-to-charge conversion using Rashba coupling at the interface between non-magnetic materials, Nat. Commun. **4**, 2944 (2013).

[18] A. Nomura, T. Tashiro, H. Nakayama, and K. Ando, Temperature dependence of inverse Rashba-Edelstein effect at metallic interface, Appl. Phys. Lett. **106**, 212403 (2015).

[19] M. B. Jungfleisch, W. Zhang, J. Sklenar, W. Jiang, J. E. Pearson, J. B. Ketterson, and A. Hoffmann, Interface-driven spin-torque ferromagnetic resonance by Rashba coupling at the interface between nonmagnetic materials, Phys. Rev. B **93**, 224419 (2016).

[20] S. Karube, K. Kondou, and Y. Otani, Experimental observation of spin-to-charge current conversion at non-magnetic metal/Bi_2O_3 interfaces, Appl. Phys. Express **9**, 033001 (2016).

[21] Y. Fan, P. Upadhyaya, X. Kou, M. Lang, S. Takei, Z. Wang, J. Tang, L. He, L. T. Chang, M. Montazeri, G. Yu, W. Jiang, T. Nie, R. N. Schwartz, Y. Tserkovnyak, and K. L. Wang, Magnetization switching through giant spin-orbit torque in a magnetically doped topological insulator heterostructure, Nat. Mater. **13**, 699 (2014).

[22] J. Han, A. Richardella, S. A. Siddiqui, J. Finley, N. Samarth, and L. Liu, Room-Temperature Spin-Orbit Torque Switching Induced by a Topological Insulator, Phys. Rev. Lett. **119**, 077702 (2017).

[23] K. Yasuda, A. Tsukazaki, R. Yoshimi, K. Kondou, K. S. Takahashi, Y. Otani, M. Kawasaki, and Y. Tokura, Current-Nonlinear Hall Effect and Spin-Orbit Torque Magnetization Switching in a Magnetic Topological Insulator, Phys. Rev. Lett. **119**, 137204 (2017).

[24] H. An, Y. Kageyama, Y. Kanno, N. Enishi, and K. Ando, Spin-torque generator engineered by natural oxidation of Cu, Nat. Commun. **7**, 13069 (2016).

[25] T. Gao, A. Qaiumzadeh, H. An, A. Musha, Y. Kageyama, J. Shi, and K. Ando, Intrinsic Spin-Orbit Torque Arising From the Berry Curvature in a Metallic-Magnet/Cu-Oxide Interface, Phys. Rev. Lett. **121**, 017202 (2018).

[26] K. U. Demasius, T. Phung, W. Zhang, B. P. Hughes, S. H. Yang, A. Kellock, W. Han, A. Pushp, and S. S. Parkin, Enhanced spin-orbit torques by oxygen incorporation in tungsten films, Nat. Commun. **7**, 10644 (2016).

[27] H. An, T. Ohno, Y. Kanno, Y. Kageyama, Y. Monnai, H. Maki, J. Shi, and K. Ando, Current-induced magnetization switching using an electrically insulating spin-torque generator, Sci. Adv. **4**, eaar2250 (2018).

[28] H. An, Y. Kanno, A. Asami, and K. Ando, Giant spin-torque generation by heavily oxidized Pt, Phys. Rev. B **98**, 014401 (2018).
[29] J. Yu, X. Qiu, W. Legrand, and H. Yang, Large spin-orbit torques in Pt/Co-Ni/W heterostructures, Appl. Phys. Lett. **109**, 042403 (2016).
[30] Q. Ma, Y. Li, D. B. Gopman, Y. P. Kabanov, R. D. Shull, and C. L. Chien, Switching a Perpendicular Ferromagnetic Layer by Competing Spin Currents, Phys. Rev. Lett. **120**, 117703 (2018).
[31] M. Morota, Y. Niimi, K. Ohnishi, D. H. Wei, T. Tanaka, H. Kontani, T. Kimura, and Y. Otani, Indication of intrinsic spin Hall effect in 4d and 5d transition metals, Phys. Rev. B **83**, 174405 (2011).
[32] H. L. Wang, C. H. Du, Y. Pu, R. Adur, P. C. Hammel, and F. Y. Yang, Scaling of Spin Hall Angle in 3d, 4d, and 5d Metals From $Y_3Fe_5O_{12}$/Metal Spin Pumping, Phys. Rev. Lett. **112**, 197201 (2014).
[33] H. Tsai, S. Karube, K. Kondou, N. Yamaguchi, F. Ishii, and Y. Otani, Clear variation of spin splitting by changing electron distribution at non-magnetic metal/Bi_2O_3 interfaces, Sci. Rep. **8**, 5564 (2018).
[34] L. Liu, T. Moriyama, D. C. Ralph, and R. A. Buhrman, Spin-torque Ferromagnetic Resonance Induced by the Spin Hall Effect, Phys. Rev. Lett. **106**, 036601 (2011).
[35] V. Ostwal, A. Penumatcha, Y.-M. Hung, A. D. Kent, and J. Appenzeller, Spin-orbit torque based magnetization switching in Pt/Cu/$[Co/Ni]_5$ multilayer structures, J. Appl. Phys. **122**, 213905 (2017).
[36] C.-F. Pai, Y. Ou, L. H. Vilela-Leão, D. C. Ralph, and R. A. Buhrman, Dependence of the efficiency of spin Hall torque on the transparency of Pt/ferromagnetic layer interfaces, Phys. Rev. B **92**, 064426 (2015).
[37] M. H. Nguyen, D. C. Ralph, and R. A. Buhrman, Spin Torque Study of the Spin Hall Conductivity and Spin Diffusion Length in Platinum Thin Films with Varying Resistivity, Phys. Rev. Lett. **116**, 126601 (2016).
[38] Y. Takeuchi, C. Zhang, A. Okada, H. Sato, S. Fukami, and H. Ohno, Spin-orbit torques in high-resistivity-W/CoFeB/MgO, Appl. Phys. Lett. **112**, 192408 (2018).
[39] K. Kondou, H. Sukegawa, S. Kasai, S. Mitani, Y. Niimi, and Y. Otani, Influence of inverse spin Hall effect in spin-torque ferromagnetic resonance measurements, Appl. Phys. Express **9**, 023002 (2016).
[40] D. Fang, H. Kurebayashi, J. Wunderlich, K. Vyborny, L. P. Zarbo, R. P. Campion, A. Casiraghi, B. L. Gallagher, T. Jungwirth, and A. J. Ferguson, Spin-orbit-driven ferromagnetic resonance, Nat. Nanotechnol. **6**, 413 (2011).
[41] J. Kim, Y.-T. Chen, S. Karube, S. Takahashi, K. Kondou, G. Tatara, and Y. Otani, Evaluation of bulk-interface contributions to Edelstein magnetoresistance at metal/oxide interfaces, Phys. Rev. B **96**, 140409(R) (2017).
[42] J. Puebla, F. Auvray, M. Xu, B. Rana, A. Albouy, H. Tsai, K. Kondou, G. Tatara, and Y. Otani, Direct optical observation of spin accumulation at nonmagnetic metal/oxide interface, Appl. Phys. Lett. **111**, 092402 (2017).
[43] F. Auvray, J. Puebla, M. Xu, B. Rana, D. Hashizume, and Y. Otani, Spin accumulation at nonmagnetic interface induced by direct Rashba–Edelstein effect, J. Mater. Sci.: Mater. Electron. **29**, 15664 (2018).
[44] M. Xu, J. Puebla, F. Auvray, B. Rana, K. Kondou, and Y. Otani, Inverse Edelstein effect induced by magnon-phonon coupling, Phys. Rev. B **97**, 180301(R) (2018).
[45] K. Kondou, H. Tsai, H. Isshiki, and Y. Otani, Efficient spin current generation and suppression of magnetic damping due to fast spin ejection from nonmagnetic metal/indium-tin-oxide interfaces, APL Mater. **6**, 101105 (2018).
[46] J. Kim, P. Sheng, S. Takahashi, S. Mitani, and M. Hayashi, Spin Hall Magnetoresistance in Metallic Bilayers, Phys. Rev. Lett. **116**, 097201 (2016).
[47] T.-C. Wang, T.-Y. Chen, C.-T. Wu, H.-W. Yen, and C.-F. Pai, Comparative study on spin-orbit torque efficiencies from W/ferromagnetic and W/ferrimagnetic heterostructures, Phys. Rev. Mater. **2**, 014403 (2018).
[48] A. G. Knapton, Alloys of platinum and tungsten, Platinum Metals Rev. **24**, 64 (1980).
[49] M. Gyoeroek, A. Kaiser, I. Sukuba, J. Urban, K. Hermansson, and M. Probst, Surface binding energies of beryllium/tungsten alloys, J. Nucl. Mater. **472**, 76 (2016).
[50] R. V. Stuart and G. K. Wehner, Energy distribution of sputtered Cu atoms, J. Appl. Phys. **35**, 1819 (1964).